

2020

Thermal Conductivity of Ultra High Molecular Weight Polyethylene: From Fibers to Fabrics

A. A. Candadai
Purdue University

J. A. Weibel
Purdue University, jaweibel@purdue.edu

A. M. Marconnet
Purdue University

Follow this and additional works at: <https://docs.lib.purdue.edu/coolingpubs>

Candadai, A. A.; Weibel, J. A.; and Marconnet, A. M., "Thermal Conductivity of Ultra High Molecular Weight Polyethylene: From Fibers to Fabrics" (2020). *CTRC Research Publications*. Paper 362.
<http://dx.doi.org/10.1021/acsapm.9b00900>

This document has been made available through Purdue e-Pubs, a service of the Purdue University Libraries.
Please contact epubs@purdue.edu for additional information.

Thermal Conductivity of Ultra High Molecular Weight Polyethylene: From Fibers to Fabrics

Aaditya A. Candadai, Justin A. Weibel, Amy M. Marconnet

Birck Nanotechnology Center and School of Mechanical Engineering, Purdue University, West Lafayette, IN 47907, USA

KEYWORDS: Ultra-high molecular weight polyethylene, thermal conductivity, infrared microscopy, heat transfer, thermally conductive fabrics

ABSTRACT: Unique combinations of properties such as mechanical compliance and chemical stability make polymers attractive for many applications. However, the intrinsic low thermal conductivity of bulk polymers has generally limited their potential for heat dissipation applications, and in fact they are widely used as thermal insulators. But in recent years, gel-spun, ultra-oriented fibers made of ultra-high molecular weight polyethylene (UHMW-PE) have sparked interest in the thermal management community due to their exceptionally high thermal conductivity. These fibers are typically used in commercially-produced protective gear such as motorcycle jackets and ballistic vests due to their high mechanical strength, but they have not been widely utilized for heat spreading and thermal management applications. While recent studies have characterized individual fibers and ultra-drawn films, the thermal properties of fabrics constructed from these materials remain virtually unexplored. Here, we synthesize plain-weave fabrics from

yarns of commercially available gel-spun UHMW-PE and measure the thermal properties of the individual microfibers, yarns, and woven fabrics using an in-house thermal characterization technique based on infrared microscopy. For the woven fabric, we report an effective in-plane thermal conductivity of $\sim 10 \text{ Wm}^{-1}\text{K}^{-1}$ in the direction aligned with the weft yarns, which is 2-3 orders of magnitude higher than conventional textile materials. This work reveals the high thermal conductivity of UHMW-PE fabrics that can be realized using a scalable textile manufacturing platform and lays the foundation for exploiting their unique thermomechanical properties for heat spreading functions in flexible/wearable devices.

1. INTRODUCTION

Polymers characteristically possess low thermal conductivity ($\sim 0.1 \text{ Wm}^{-1}\text{K}^{-1}$) and are often used for thermal insulation in various applications [1-3]. Their low thermal conductivity primarily arises from intrinsic defects and molecular chain entanglements present in their structures [4]. However, with the innovation of gel-spinning processes, high-performance polymer fibers are now commercially produced in large volume to achieve greatly enhanced mechanical strength and modulus as compared to conventional bulk polymers [5,6]. This enhancement is primarily a result of increased crystallinity and orientation which also leads to improved thermal properties [7-10]. Gel-spun, ultra-high molecular weight polyethylene (UHMW-PE) has two orders of magnitude higher thermal conductivity as compared to that of bulk polyethylene ($0.2\text{-}0.5 \text{ Wm}^{-1}\text{K}^{-1}$) [11-13]. This approach of enhancing the intrinsic thermal conductivity of polymers is advantageous compared to traditional methods of introducing high-conductivity fillers in a polymer matrix, where the interfacial thermal resistance between the two components significantly limits conductivity enhancement [14]. Even when the interfacial resistances are significantly reduced

with proper surface functionalization, it is not clear if a thermal percolation threshold can be achieved, and so the effective thermal conductivity of the composite is still limited by the thermal transport through the matrix [15-17].

Many studies in the literature have focused on thermal characterization of UHMW-PE materials [18-28], as summarized in Fig. 1, of different forms including fibers, thin film, and yarns. As seen from this chart, there is spread in the reported thermal conductivity for a given form, possibly depending on the measurement technique employed or variations in the fabrication process. Choy *et al.* [18] fabricated fiber-reinforced composite sheets having differing fiber volume fractions; low-density PE was reinforced with commercial gel-spun polyethylene fibers (Spectra). The thermal conductivity of the individual fibers was estimated to be $\sim 38 \text{ Wm}^{-1}\text{K}^{-1}$ by extrapolating laser-flash measurements of the composite sheets to a volume fraction of 1. Fujishiro *et al.* [19,20] characterized fiber bundles made up of 6000 monofilaments of commercial UHMW-PE fiber (Dyneema) (at temperatures below 260 K) using both a direct steady state method to measure thermal conductivity and a transient technique to measure thermal diffusivity. Their measurements reported thermal conductivities of up to $60 \text{ Wm}^{-1}\text{K}^{-1}$ for the bundles. Wang *et al.* [21] measured a thermal conductivity of $\sim 15 \text{ Wm}^{-1}\text{K}^{-1}$ for individual commercial microfibers (Dyneema) using time-domain thermoreflectance experiments. The thermal conductivity of the same type of microfibers was measured to be $\sim 23 \text{ Wm}^{-1}\text{K}^{-1}$ using the transient electrothermal technique employed by Liu *et al.* [22]. More recently, Shen *et al.* [23] performed AFM tip-based thermal measurements to demonstrate that a thermal conductivity of up to $\sim 104 \text{ Wm}^{-1}\text{K}^{-1}$ can be achieved for gel-spun and ultra-drawn PE nanofibers with diameters on the order of $\sim 100 \text{ nm}$. In other recently reported studies by Xu *et al.* [24], Ghasemi *et al.* [25], and Ronca *et al.* [26], ultra-oriented,

thin PE films ($\sim 1-10 \mu\text{m}$) have been fabricated using very high draw ratios to achieve thermal conductivities of $16-65 \text{ Wm}^{-1}\text{K}^{-1}$.

The potential to leverage advantages such as mechanical compliance and flexibility offered by polymers in comparison to metals, with the metal-like thermal conductivity of UHMW-PE, combined with its chemical stability, electrically insulating properties, and light weight make it very attractive for applications such as a heat spreader in flexible/wearable electronic devices. Such potential thermal management applications require a high effective thermal *conductance*, for which both thermal conductivity of the material and the available cross-sectional area for heat flow are important. The thermal conductance of thin films, such as those fabricated in recent studies [24-26], is limited by the very small final thicknesses intrinsic to the ultra-drawing process required to produce a material with high thermal conductivity. There is an evident need to scale up high-thermal-conductivity PE materials to bulk sizes having large cross sections for heat flow, but while maintaining their desirable thermal properties.

Construction of flexible fabrics from UHMW-PE fibers is very promising for these applications as textile manufacturing processes are scalable to large areas and high volumes. But, scaling up of the material from individual microfibers to yarns and ultimately to fabrics introduces numerous material interfaces, volume-fraction considerations and associated thermal resistances which are expected to play a critical role in determining the effective heat transfer behavior. Thus, a systematic study of the effective thermal conductivity of UHMW-PE spanning across these different forms and length scales is crucial to understanding and assessing the potential of fabrics for thermal management applications. To the best of our knowledge, no studies in the literature have reported thermal characterization of fabrics constructed from UHMW-PE fibers.

In this work, we experimentally characterize the thermal conductivity of UHMW-PE fibers, yarns formed from twisting these fibers, and woven fabrics. Plain-weave type fabrics (see Fig. 2) are constructed from UHMW-PE yarns with a relatively higher density of yarns along one direction of the fabric. In order to enable multi-scale thermal characterization of the different forms of UHMW-PE, we develop an in-house steady-state thermal conductivity measurement method based on infrared microscopy. Using this simple technique, in which an electrified wire heats up an orthogonally oriented contacting specimen via Joule heating, we can extract the thermal conductivity of these specimens of drastically different sizes and forms without the need for estimating the thermal contact resistance between the heater wire and the sample. This is attributed to the simultaneous capture of two-dimensional steady-state temperature maps of the heater wire and the sample, as well as tuning of the size of the heater wire to be the same order as thermal conductance of the sample being measured. An associated one-dimensional heat transfer model that incorporates the effect of radiation losses is used to ultimately quantify the thermal conductivity of the sample. We measure the axial thermal conductivity of the fibers and yarns, and the in-plane effective thermal conductivity of the fabric in the dominant heat conduction direction. Our findings help understand the effective thermal behavior as a function of scaling-up the high conductivity fibers, and indicate very promising thermal properties for the woven fabrics for applications as a flexible/wearable heat spreader. In addition, we also develop a reduced-order heat conduction model to estimate the effective in-plane thermal conductivity of plain-weave fabrics, which serves as a simple confirmation of the key conclusions from our experimental data.

2. EXPERIMENTAL METHODS

2.1 Material Details and Sample Preparation: The UHMW-PE material used in this study was acquired in the form of a flat yarn (DSM Dyneema SK75; Atkins and Pearce Inc.) with a linear

density of 0.044 g/m. The fibers in the flat yarn are twisted together using a drop spindle tool which produces a well-bound twisted yarn (see Fig. 2) that is suitable for weaving.

The twisted yarns are used to construct a swatch of woven fabric on a miniature weaving loom (Wee Weaver; Purl & Loop) with a gauge specification of 12 grooves per inch. The warp yarn is first wound through the grooves on both ends of the loom and held taut. The weft yarn is interlaced over and under each successive row (thread) of warp yarn, as illustrated in Fig. 2a, and then is similarly interlaced back through the fabric in the opposite direction after it passes through the last warp thread. Successive rows of weft threads are compressed together such that the weft number density is \sim 4-5 times that of the warp. Ultimately, a plain-weave fabric pattern with a high density of threads in the weft direction (*i.e.*, weft-faced weave) is constructed, as seen in the photographs and optical microscope image in Fig. 2c and 2d.

Thermal measurements are performed for individual fibers pulled out from the flat yarns, twisted yarns, and the woven fabric. For the fabric samples, thin strips of material must be cut without fraying of the fabric. Fabric strips \sim 2 cm long (parallel to the weft) and \sim 2.5 mm wide are cut using a CO₂ laser (ULS PLS6MW) while the fabric is held under tension in the loom. This fuses the cut edges of the strips and prevents unraveling of the yarns. We note that the width of the fused region is very small compared to the width of the fabric and does not influence the thermal measurements for the fabric strip.

2.2 Thermal Characterization Metrology: The thermal measurements are performed using an infrared (IR) microscope system (Infrascop; Quantum Focus Instruments Corporation) which has a pixel resolution of 12.2 μ m at 1 \times magnification and a temperature resolution of \sim 0.1 $^{\circ}$ C, although the absolute accuracy of the temperature measurements depends on emissivity calibration (see S1.1 in Supporting Information for details). Schematic drawings of the experimental setup are

shown in Fig. 3a. The sample to be characterized is suspended across the middle of an annular-ring-shaped heat sink (~ 1 cm inner diameter). A nichrome wire is suspended orthogonally across the heat sink and contacts the center of the sample. The wire is heated via Joule heating by supplying electric current using a DC source meter (Keithley 2420). Some portion of the heat generated in the wire is conducted in the wire both to the sink at either end and to the center, where the sample is attached, establishing a non-linear temperature profile in the wire at steady state. In the sample, heat is conducted from the central point of contact with the wire to the sink at both ends; at steady state, this establishes a linear temperature gradient in both halves of the sample. This wire-sample cross-structure assembly is placed inside a vacuum chamber (Linkam Scientific Instruments TS1500V) which is connected to a two-stage turbo pump (Varian TPS Bench-9698215) that maintains a pressure of $\sim 1 \times 10^{-5}$ mbar inside the chamber. This minimizes convective heat loss from the wire and the sample to the ambient.

Considering a control volume around the central contact region between the wire and the junction, as shown in Fig. 3b, we define Q_L and Q_R as the heat rates entering this control volume through the wire, and Q_T and Q_B as the heat rates leaving this control volume through the sample. There is also heat generation in the central region of the wire within the control volume, $Q_{gen} = I^2 R_l c$, where I is the current supplied to the wire, R_l is the measured electrical resistance per unit length of the wire, and c is the length of the wire within the control volume. From an energy balance in this control volume,

$$Q_L + Q_R + Q_{gen} = Q_T + Q_B. \quad (1)$$

The heat rates Q_T and Q_B can be related to the temperature gradients in the wire using Fourier's law assuming the heat transfer in the sample is governed by one-dimensional heat conduction. This is a good assumption because the experiments are conducted in vacuum and the maximum

temperature rise is limited to ~10 K to minimize radiation effects, and this is confirmed by the observed linear temperature profile in the sample regions. However, depending on the thermal conductivity and dimensions of the sample being measured, in some cases the radiation losses from the sample need to be considered to obtain an accurate measurement of sample thermal conductivity (see S1.2 in Supporting Information for details). Considering one-dimensional heat conduction in the sample to be valid, conduction within each sample region is governed by Fourier's law and calculated as

$$Q_T + Q_B = k_s A_s \left. \frac{dT}{dy} \right|_T + k_s A_s \left. \frac{dT}{dy} \right|_B, \quad (2)$$

where k_s and A_s are the thermal conductivity and cross-sectional area of the sample, respectively. Therefore, the sample thermal conductivity can be determined using the relationship below if the associated heat rates and temperature gradients can be measured:

$$k_s = \frac{Q_L + Q_R + Q_{gen}}{A_s \left\{ \left. \frac{dT}{dy} \right|_T + \left. \frac{dT}{dy} \right|_B \right\}}. \quad (3)$$

Note that, in general, radiation losses from the wire region inside the control volume are very small compared to the total heat rate, $Q_L + Q_R + Q_{gen}$ (see also S1.2 of the Supporting Information for more details). However, radiation is important in the section of the heater wire that is not in contact with the sample as discussed in the following section.

A unique feature of this analysis is that the measurement of thermal conductivity is independent of the thermal contact resistance between the heater wire and the sample, because the heat flow from the wire to the sample is extracted directly, as is the temperature profile in the sample. The process of extracting the heat rates and sample temperature gradients from the IR measurements is illustrated in Fig. 3c. The temperature profiles of both the wire and the sample are determined from the steady state IR temperature map at a given value of input current. Note that extraction of

the temperature profiles is performed based on the calibrated emissivity values of the wire and the sample, which are performed *ex situ* prior to the actual experiments (see S1.1 in Supporting Information). For all experiments, the nichrome wire is coated black with a colloidal graphite solution to reduce its reflectivity. The linear temperature gradients $\left.\frac{dT}{dy}\right|_T$ and $\left.\frac{dT}{dy}\right|_B$ are calculated from the slope of the measured profiles. In the suspended region of the heater wire on each side of the sample, the heat transfer is governed by conduction in the wire and radiation to the surroundings, which is important due to the relatively high wire temperatures. The following energy equation dictates the wire temperature profile (expressed here for the right side only):

$$\frac{\partial^2 T}{\partial x^2} - \frac{h_r P (T - T_{sur})}{k_w A} + \frac{q'''}{k_w} = 0 \quad (4)$$

$$x = \ell: T = T_0 \quad (5)$$

$$x = 0: kA \left.\frac{dT}{dx}\right| = Q_R. \quad (6)$$

Here, k_w is the wire thermal conductivity, h_r is the linearized radiation heat transfer coefficient, T_{sur} is the temperature of the surroundings, P is the wire perimeter, A is the wire cross-sectional area, q''' is the heat generation rate in the wire ($q''' = (I^2 R_l)/A$), ℓ is the length of the wire on the right side of the sample, and T_0 is the measured temperature boundary condition from the IR temperature map. Solving this differential equation, the temperature profile in the right-side of the wire is of the form

$$\begin{aligned} T(x) = & \frac{e^{-mx}}{m^2 k_w A (e^{2m\ell} + 1)} (Ae^{m(2x+\ell)} \{m^2 k_w (T_0 - T_{sur}) - q'''\}) \\ & + Ae^{m(2\ell+x)} \{m^2 k_w T_{sur} + q'''\} - mQ_R e^{2m\ell} + mQ_R e^{2mx} \\ & + Ae^{m\ell} \{m^2 k_w (T_0 - T_{sur}) - q'''\} + Ae^{mx} \{m^2 k_w T_{sur} + q'''\}, \end{aligned} \quad (7)$$

where $m^2 = (h_r P)/(k_w A)$. The thermal conductivity of the wire, k_w is determined from a separate calibration experiment performed by heating the wire in the absence of the sample [29] (also see S1.3 in Supporting Information). This leaves the heat flow rate in the right side of the wire, Q_R as the only unknown parameter in Eq. 7, which is fit to the measured IR temperature profile using a least squares algorithm. Analogous expressions are valid on the left side of the wire and Q_L is extracted in the same manner. Finally, with all terms in Eq. 3 known, the thermal conductivity of the sample is calculated. Details of the uncertainty/sensitivity of the described measurement technique are presented in our recent work [29].

To validate the experimental approach, we characterize reference samples having known thermal conductivity using the developed metrology technique. Two different materials are chosen because they have a similar geometry as the yarn and fabric samples: a nichrome wire (circular cross-section similar to the yarn) and a bulk HDPE film (rectangular cross-section) of width comparable to the fabric sample. Details of these validation experiments are presented in the Supporting Information (see S2). We note that a very good agreement ($\sim 10\%$ difference) is obtained between the experimentally measured values and the actual thermal properties of the reference materials.

3. RESULTS AND DISCUSSION

We present the infrared thermal characterization results of the Dyneema yarn followed by the woven fabric. Our measurements reveal that an in-plane effective thermal conductivity on the order of $10 \text{ Wm}^{-1}\text{K}^{-1}$ is achieved for the fabric along the dominant heat conduction direction which is along the weft yarns of the fabric. The trends in effective thermal conductivity as the material is scaled from fibers to yarns to fabric are explained using reduced-order thermal models. Finally, we compare the key findings of this work with related studies on UHMW-PE materials.

3.1. Thermal Characterization of Yarns. A yarn sample with an effective diameter of ~ 370 μm is mounted on the heat sink inside the vacuum chamber such that the nichrome heating wire is threaded through the fibers of the bundle to obtain more uniform heating throughout the yarn cross-section. Fig. 4a shows an example IR temperature map obtained from the measurements in the wire–yarn cross-structure arrangement. Two different temperature maps are obtained at each level of supplied current, one based on the calibrated emissivity of the wire (in the wire region), and the other based on the calibrated emissivity of the yarn (in the yarn region). These are analyzed to fit for the heat rates Q_L , Q_R , and the temperature gradients in the yarn as shown in Fig. 4b. The heat generation in the junction region of the wire Q_{gen} is also calculated to determine the total heat flux flowing into the yarn sample. This is repeated at five different levels of supplied current. Because the total heat flux ($\{Q_L + Q_R + Q_{gen}\}/A_s$) at each power level is linearly proportional to the sum of the temperature gradients ($|dT/dy|_T + |dT/dy|_B$) on each side (see Eq. 3), a single value of thermal conductivity is obtained from the measured slopes by fitting the experimental data to a straight line passing through origin, as shown in Fig. 4c. This procedure reduces the measurement uncertainty associated with the experiments. Given the nominal values of all input parameters to the model (e.g., diameter, emissivity, etc.), the thermal conductivity of the yarn (Dyneema SK75) is determined to be $15.8 \pm 0.7 \text{ Wm}^{-1}\text{K}^{-1}$ for a first sample and 16.3 ± 0.7 and $16.4 \pm 0.7 \text{ Wm}^{-1}\text{K}^{-1}$ for two repeated trials of a second sample. As illustrated in Fig. 4c, the thermal conductivity values measured from the two trials using the second yarn sample are in excellent agreement, indicating good repeatability.

Based on previous studies related to yarn structures [30-32], we note that the level of yarn twist and orientation of fibers within the yarn are important factors that could influence the effective properties of the yarn. With increase in yarn twist, two key mechanisms may affect the heat

conduction behavior: (i) increased effective packing of the fibers within the yarn due to compaction, which would lead to an increase in the yarn effective thermal conductivity; and (ii) an increased length of individual fibers per unit of apparent axial conduction length (*i.e.*, an extended path-length for heat conduction following the spiral of the fiber), which leads to a decrease in the yarn effective thermal conductivity. A decrease in yarn thermal conductivity with increasing twist was predicted in [30] by considering the varying helix angle of fibers from the core to the surface of the yarn for an assumed packing arrangement. However, this model only accounts for the increased conduction length due to the oblique orientation of the fibers with respect to the principal yarn axis, without considering the effect of increased compaction [31, 32]. In the present study, we perform thermal measurements with the twisted yarns to explore the effect of yarn twist on the effective thermal conductance (per unit length) of the yarn. Note that the yarn effective thermal conductance per unit length (with units of WmK^{-1}) is defined as the product of the effective thermal conductivity and the yarn cross-sectional area. This parameter is of interest for fabric construction because it directly influences the in-plane effective thermal properties of fabrics woven from the twisted yarns. The effective thermal conductance can be easily extracted from our measurements without having to consider changes in the effective yarn cross-sectional area at different twist levels. We investigate the effect of yarn twist by performing the IR experiments for four different twist levels characterized by the average surface helix angle of the yarn, as illustrated in Fig. 5a. The extracted thermal conductance, increases by only $\sim 6\%$ from the lowest to the highest twist level considered here, spanning a surface helix angle change of about $\sim 20^\circ$, as shown in Fig. 5b. We conclude from these experiments that the change in yarn thermal conductance is not significant for the range of twist levels characterized here, which is also representative of the twist level of the yarns in the constructed woven fabric.

3.2. Thermal Characterization of Fabrics. A strip of woven fabric having a width of ~ 2.1 mm and thickness of ~ 660 μm is characterized. In order to achieve uniform heating across the fabric thickness and obtain good thermal contact conductance with the heating wire under vacuum conditions, a small piece of copper tape is wound around the fabric in the contact region and a thermal gap pad is placed between the wire and the fabric sample. A schematic drawing of this experimental configuration for fabric testing has been included in the Supporting Information (section S1.4) for clarity. The thermal gap pad helps in conducting a greater amount of heat into the sample at a given level of electrical power input, but does not influence the measured sample thermal conductivity. A representative IR temperature map for the wire–fabric experiment is shown in Fig. 6a and the corresponding temperature profiles of the wire and the fabric in Fig. 6b. For the fabric, a sharp dip in the wire temperature profile is observed on either side of the contact region, which contrasts the wire temperature profile seen for the yarn test in Fig. 4b. This occurs due to the larger amount of heat being removed by the fabric sample due to its higher thermal conductance as compared to the yarn sample. Analogous to the analysis for the yarn, the total heat flux flowing into the fabric, and the temperature gradients in the fabric region, are obtained for each level of input electrical power. The effective thermal conductivity of the fabric is extracted from the linear fit shown in Fig. 6c. The radiation losses from the control volume in the central region of the wire are verified to be negligible ($\sim 1\%$) compared to the total heat rate, $Q_L + Q_R + Q_{gen}$.

The effective thermal conductivity of the fabric is determined to be $9.5 \pm 0.6 \text{ Wm}^{-1}\text{K}^{-1}$ based on the two experimental trials shown in the Fig. 6c. The first trial (Run 1) is performed with the thermal gap pad placed in between the wire and the fabric to enhance thermal conductance at the junction, while the second trial (Run 2) is performed without the use of this pad. The results from

these two independent runs yield the same value of thermal conductivity to within measurement uncertainty, which further demonstrates that the developed characterization technique is independent of the junction thermal contact resistance.

In order to obtain an estimate of effective fabric thermal conductivity to compare with our experimental results, and to also understand the effect of yarn density on fabric conductivity, we have developed a reduced-order heat conduction model. In this model, a full nodal-network-based analysis (see details in S3 of Supporting Information) similar to the approach implemented for modeling conduction through foam structures in [33] is performed. Effective fabric thermal conductivity along a given direction of interest is calculated by assigning constant temperature boundary conditions T_H and T_C to the associated opposite fabric ends, while insulating the other two sides as shown in Fig. 7a. This modeling analysis demonstrated that for a plain-weave fabric, the effective thermal conductivity in the direction under consideration is independent of the inter-yarn thermal contact resistance at the nodal locations, because the yarns oriented perpendicular to the direction of heat flow (along x as seen in Fig. 7a) are insulated at their end and therefore non-participating. As a result, an inter-yarn thermal contact resistance between orthogonal yarns does not need to be specified in this case.

Based on the results from the reduced-order model, the effective fabric thermal conductivity of the plain-weave fabric is dependent on three model input parameters: the yarn thermal conductivity (k_y), the center-to-center spacing between adjacent parallel yarns (l_y), and the effective yarn diameter (d_y). The schematics in Fig. 7b portray the effective cross-sections of a fabric with a high packing density ($l_y/d_y = 0.5$) and low packing density ($l_y/d_y = 1$) of yarns parallel to the heat flow direction. From this model, the effective thermal conductivity is determined to be directly proportional to the cross-sectional area-based packing fraction of the yarns oriented along

the direction of heat flow. Specifically, as illustrated in the plot in Fig. 7c, the effective fabric thermal conductivity is inversely proportional to l_y/d_y for a given value of k_y , which is taken to be $16 \text{ Wm}^{-1}\text{K}^{-1}$ based on the results obtained from the yarn characterization experiments. From inspection of the images of the woven fabric shown in Fig. 2d, a value of $l_y/d_y \sim 0.5\text{-}0.6$ is representative of the experimentally characterized woven fabric. At this packing density, the estimate of effective fabric conductivity from the reduced-order model matches well with the result from the thermal characterization experiment, as shown in Fig. 7c. Further, the results obtained from the reduced-order model also offer quantitative understanding of the effect of yarn packing in the fabric weave on effective fabric thermal conductivity.

3.3. Discussion. The results from the thermal characterization study presented in the previous sections indicate a very high measured thermal conductivity for UHMW-PE yarns and fabrics, especially considering that these are constructed out of polymer fibers. To interpret these measured thermal conductivities, we have also characterized the individual fibers (monofilaments with diameter $\sim 20 \mu\text{m}$) that comprise the yarn and fabric. These experiments are performed using a higher magnification IR lens in order to achieve the required spatial and temperature resolution (fiber measurement details are in S4 of the Supporting Information). The thermal conductivity of these fibers is measured to be $\sim 25\text{-}30 \text{ Wm}^{-1}\text{K}^{-1}$.

Consider the thermal conductivity of oriented UHMW-PE as the material is scaled from fibers to fabrics, as illustrated in Fig. 1a. Our measurements in this work reveal that the effective thermal conductivity of UHMW-PE only reduces by a factor of ~ 3 as microfibers are scaled up to woven fabrics. This reduction is attributed mainly to the packing density of individual fibers within a yarn, and the packing density of yarns within a fabric. The effective density of yarns, based on measuring the yarn linear density and assuming a circular cross-section, is determined to be ~ 460

kg/m³, which is lower than the specified density of an individual fiber by a factor of ~2. This is the same factor of reduction in effective thermal conductivity from fibers to yarns as measured. Further, the results from the reduced-order fabric thermal conductivity model explain this same reduction due to packing density from the yarns to the woven fabric. Nevertheless, given these fabrics are a macroscale material, their effective thermal conductivity (~10 Wm⁻¹K⁻¹) is remarkable compared to a bulk form of polyethylene (~0.5 Wm⁻¹K⁻¹ for HDPE).

Comparing to the values in literature, as apparent from Fig. 1, our measured thermal conductivity of the individual fibers is generally in good agreement with other studies [21,22]. The thermal conductivity of fiber bundles measured in [19] are much higher compared to our measurement for the yarns. However, we note that radiation losses and parasitic conduction losses were not considered in the conventional steady-state measurement technique used in this previous study [19], which would tend to overestimate the thermal conductivity. Further, as pointed out in [21], the value of thermal conductivity directly measured for the fiber bundle (~60 Wm⁻¹K⁻¹) in [19] does not agree with the thermal conductivity extracted from the thermal diffusivity measurement (~36 Wm⁻¹K⁻¹) in the same work [19], as well as with that extrapolated from the measurement of the fiber-reinforced plastic (in [19]) comprising of the same fibers (~33 Wm⁻¹K⁻¹). Our measurements for yarns also corroborate the measurements of individual microfibers [18,21,22], as a reduction in effective conductivity (and not an increase) is expected for yarns when compared to individual fibers due to a decrease in effective density.

Fig.1 also indicates that ultra-drawn oriented thin films [24,25] can have a similar thermal conductivity to individual fibers. The recent study by Xu *et al.* [24] demonstrates great potential for scalability of these films along the drawing direction, but the drawing process required to obtain such high thermal conductivity also greatly reduces the thickness. Therefore, even though the

thermal conductivity of the fabricated films increases from $0.38 \text{ Wm}^{-1}\text{K}^{-1}$ to $62 \text{ Wm}^{-1}\text{K}^{-1}$ as the draw ratio increases to 110, the thermal conductance (per unit length) of these films across all draw ratios is limited to relatively low values in the range of $2.9 \times 10^{-7} \text{ WmK}^{-1}$ to $3.9 \times 10^{-7} \text{ WmK}^{-1}$. To address this scalability limit in the thickness direction, Xu *et al.* [24] also demonstrated construction of a $150 \text{ }\mu\text{m}$ -thick laminate by hot-pressing many films produced at a high draw ratio of 50, and measured the in-plane thermal conductivity of the laminate to be $\sim 33 \text{ Wm}^{-1}\text{K}^{-1}$. The thermal conductance of this fabricated 100-layer laminate ([in 24]) is $\sim 5 \times 10^{-6} \text{ WmK}^{-1}$, while the conductance of the single-layer woven fabric test strip (from this work) is $1.3 \times 10^{-5} \text{ WmK}^{-1}$. The woven fabric strip has a thermal conductance 2.6 times greater primarily due to its higher length scale compared to the film laminate. We note that while the high thermal conductivity of the laminate is very promising for heat spreading applications, effective scaling-up of these structures while maintaining these properties is crucial for such applications. The ultra-drawing process constrains the cross-sections that can be achieved for the produced films, whereas single-layer weaves can easily be scaled along the width and length directions. Also, laminates of larger thickness prepared in this manner may be stiffer as compared to woven materials which can potentially limit their usage in flexible device applications.

Based on the results of the current study, woven fabrics show great promise for scalable fabrication of a high effective thermal conductivity material because weaves with lengths and widths on the order of meters, and thicknesses on the order of $\sim 0.5\text{-}1 \text{ mm}$, can easily be produced by a large-scale textile manufacturing process. Further, the in-plane thermal conductivity of UHMW-PE fabrics is more than two orders of magnitude higher than conventional fabrics such as cotton ($0.03\text{-}0.07 \text{ Wm}^{-1}\text{K}^{-1}$), silk ($0.09 \text{ Wm}^{-1}\text{K}^{-1}$), and wool ($0.04 \text{ Wm}^{-1}\text{K}^{-1}$) [34-36]. Therefore, UHMW-PE fabrics are ideally suited to wearables and other flexible device applications where

good heat spreading functionality is desired. Additionally, complex weaves and multi-layer fabric stacks provide an avenue to tailor the high thermal conductivity of these materials to a particular application.

4. CONCLUSIONS

In this study, we have explored the effective heat conduction properties of UHMW-PE in the forms of microfibers, yarns, and woven fabrics. To characterize these materials spanning across length scales from a few microns to hundreds of millimeters, we have developed a steady-state thermal metrology technique based on simple energy balance principles using IR microscopy. The technique has been validated using reference materials, and a reduced-order thermal model has also been developed to corroborate our experimental data which shows that macroscale woven polymer fabrics made of high conductivity UHMW-PE fibers exhibit an in-plane effective thermal conductivity on the order of $10 \text{ Wm}^{-1}\text{K}^{-1}$. Through this study, we have demonstrated that textile weaving, being a well-established mass-manufacturing process, is a promising method to scale up UHMW-PE microfibers into a bulk material having high thermal conductivity. Given the rapid advancements being made in the field of wearable device technology, flexible polymer-based high thermal conductivity materials can address the growing need for thermal management solutions that address ergonomics-driven thermal constraints. Based on the findings of this study, we believe that thermally conductive UHMW-PE fabrics offer great potential for such heat spreading applications.

ASSOCIATED CONTENT

Supporting Information. The Supporting Information is available free of charge on the ACS Publications website at DOI:

Infrared Thermal Measurement Technique, Thermal Metrology Validation Experiments,
Reduced-Order Fabric Thermal Model, Ultra High Molecular Weight Polyethylene Fiber
Thermal Characterization (PDF)

AUTHOR INFORMATION

Corresponding Authors

*Email: marconnet@purdue.edu (A.M.M.), jaweibel@purdue.edu (J.A.W.)

Notes

The authors declare no competing financial interest.

ACKNOWLEDGMENTS

The authors thank the industry members of the Cooling Technologies Research Center, a graduated National Science Foundation Industry/University Cooperative Research Center at Purdue University, for providing funding support for this work. The authors appreciate Prof. Ali Shakouri (Purdue University) for providing access to the vacuum pump and stage; Prof. Alison Stewart-Guinee (Purdue University) for useful conversations and guidance on weaving of fabrics; Srivathsan Sudhakar (Purdue University) for help with laser-cutting of the fabrics; and Radhakrishan Korlam (IIT Madras; Purdue University) for inputs related to the reduced-order packing model.

REFERENCES

1. Choy, C. L. Thermal Conductivity of Polymers. *Polymer* **1977**, *18*, 984-1004.
2. Sperling, L. H. Introduction to Physical Polymer Science. *New York: Wiley* **2006**, 78.

3. Tant, M. R.; Connell, J. W.; McManus, H. L. High-Temperature Properties and Applications of Polymeric Materials. *Washington, DC: American Chemical Society* **1995**.
4. Chae, H. G.; Kumar, S. Making Strong Fibers. *Science* **2008**, *319*, 908-909.
5. Adams, W. W.; Eby, R. K. High-Performance Polymer Fibers. *MRS Bulletin* **1987**, *12*, 22-26.
6. Smith, P.; Lemstra, P. J.; Kalb, B.; Pennings, A. J. Ultrahigh-strength Polyethylene Filaments by Solution Spinning and Hot Drawing. *Polymer Bulletin* **1979**, *1*, 733-736.
7. Park, J. H.; Rutledge, G. C. Ultrafine High-Performance Polyethylene Fibers. *J. Mater. Sci.* **2018**, *53*, 3049-3063.
8. Choy, C. L.; Chen, F. C.; Luk, W. H. Thermal Conductivity of Oriented Crystalline Polymers. *J. Polym. Sci.* **1980**, *18*, 1187–1207.
9. Choy, C. L.; Young, K. Thermal Conductivity of Semi-Crystalline Polymers—A Model. *Polymer* **1977**, *18*, 769– 776.
10. Yamanaka, A.; Takao, T. Thermal Conductivity of High-Strength Polyethylene Fiber and Applications for Cryogenic Use. *ISRN Mater. Sci.* **2011**.
11. Mergenthaler, D. B.; Pietralla, M.; Roy, S.; Kilian, H.G. Thermal Conductivity in Ultraoriented Polyethylene. *Macromolecules* **1992**, *25*, 3500-3502.
12. Vasileiou, A. A.; Kontopoulou, M.; Docoslis, A. A. Noncovalent Compatibilization Approach to Improve the Filler Dispersion and Properties of Polyethylene/Graphene Composites. *ACS Appl. Mater. Interfaces* **2014**, *6*, 1916–1925.

13. Haggemueller, R.; Guthy, C.; Lukes, J. R.; Fischer, J. E.; Winey, K. I. Single Wall Carbon Nanotube/Polyethylene Nanocomposites: Thermal and Electrical Conductivity. *Macromolecules* **2007**, *40*, 2417– 2421.
14. Huxtable, S. T.; Cahill, D. G.; Shenogin, S.; Xue, L.; Ozisik, R.; Barone, P.; Usrey, M.; Strano, M. S.; Siddons, G.; Shim, M.; Koblinski, P. Interfacial Heat Flow in Carbon Nanotube Suspensions. *Nat. Mater.* **2003**, *2*, 731.
15. Kargar, F.; Barani, Z.; Salgado, R.; Debnath, B.; Lewis, J. S.; Aytan, E.; Lake, R. K.; Balandin, A. A. Thermal Percolation Threshold and Thermal Properties of Composites with High Loading of Graphene and Boron Nitride Fillers. *ACS Appl. Mater. Interfaces* **2018**, *10*, 37555-37565.
16. Shenogina, N.; Shenogin, S.; Xue, L.; Koblinski, P. On the Lack of Thermal Percolation in Carbon Nanotube Composites. *Appl. Phys. Lett.* **2005**, *87*, 133106.
17. Li, A.; Zhang, C.; Zhang, Y. F. Thermal Conductivity of Graphene-Polymer Composites: Mechanisms, Properties, and Applications. *Polymers* **2017**, *9*, 437.
18. Choy, C. L.; Fei, Y.; Xi, T. G. Thermal conductivity of Gel-Spun Polyethylene Fibers. *J. Polym. Sci. Part B: Polym. Phys.* **1993**, *31*, 365-370.
19. Fujishiro, H.; Ikebe, M.; Kashima, T.; Yamanaka, A. Thermal Conductivity and Diffusivity of High-Strength Polymer Fibers. *Jap. J. Appl. Phys.* **1997**, *36*, 5633.
20. Fujishiro, H.; Ikebe, M.; Kashima, T.; Yamanaka, A. Drawing Effect on Thermal Properties of High-Strength Polyethylene Fibers. *Jap. J. Appl. Phys.* **1998**, *37*, 1994.

21. Wang, X.; Ho, V.; Segalman, R. A.; Cahill, D. G.; Thermal Conductivity of High-Modulus Polymer Fibers. *Macromolecules* **2013**, *46*, 4937-4943.
22. Liu, J.; Xu, Z.; Cheng, Z.; Xu, S.; Wang, X. Thermal Conductivity of Ultrahigh Molecular Weight Polyethylene Crystal: Defect Effect Uncovered by 0 K Limit Phonon Diffusion. *ACS Appl. Mater. Interfaces* **2015**, *7*, 27279-27288.
23. Shen, S.; Henry, A.; Tong, J.; Zheng, R.; Chen, G. Polyethylene Nanofibres with Very High Thermal Conductivities. *Nat. Nanotechnol.* **2010**, *5*, 251.
24. Xu, Y.; Kraemer, D.; Song, B.; Jiang, Z.; Zhou, J.; Loomis, J.; Wang, J.; Li, M.; Ghasemi, H.; Huang, X.; Li, X. 2019. Nanostructured Polymer Films with Metal-Like Thermal Conductivity. *Nat. Commun.* **2019**, *10*, 1771.
25. Ghasemi, H.; Thoppey, N.; Huang, X.; Loomis, J.; Li, X.; Tong, J.; Wang, J.; Chen, G. High Thermal Conductivity Ultra-High Molecular Weight Polyethylene (UHMWPE) Films. *Intersociety Conference on Thermal and Thermomechanical Phenomena in Electronic Systems (IEEE ITherm)* **2014**, 235-239.
26. Ronca, S.; Igarashi, T.; Forte, G.; Rastogi, S. Metallic-Like Thermal Conductivity in a Lightweight Insulator: Solid-State Processed Ultra High Molecular Weight Polyethylene Tapes and Films. *Polymer* **2017**, *123*, 203-210.
27. Zhu, B.; Liu, J.; Wang, T.; Han, M.; Valloppilly, S.; Xu, S.; Wang, X. Novel Polyethylene Fibers of Very High Thermal Conductivity Enabled by Amorphous Restructuring. *ACS Omega* **2017**, *2*, 3931-3944.

28. Poulaert, B.; Legras, R.; Chielens, J. C.; Vandenhende, C.; Issi, J. P. Thermal-Conductivity of Highly Oriented Polyethylene Fibers. *Polymer Communications* **1990**, *31*, 148.
29. Candadai, A. A.; Weibel, J. A.; Marconnet A. M. A Measurement Technique for Thermal Conductivity Characterization of Ultra-High Molecular Weight Polyethylene Yarns Using High-Resolution Infrared Microscopy. *Intersociety Conference on Thermal and Thermomechanical Phenomena in Electronic Systems (IEEE ITherm)* **2019**.
30. Rengasamy, R.S.; Kawabata, S. Computation of Thermal Conductivity of Fibre from Thermal Conductivity of Twisted Yarn **2002**.
31. Shah, D. U.; Schubel, P. J.; Licence, P.; Clifford, M. J. Determining the Minimum, Critical and Maximum Fibre Content for Twisted Yarn Reinforced Plant Fibre Composites. *Comp. Sci. Technol.* **2012**, *72*, 1909-1917.
32. Pan, Ning. Development of a Constitutive Theory for Short Fiber Yarns: Part III: Effects of Fiber Orientation and Bending Deformation. *Textile Research Journal* **1993**, *63*, 565-572.
33. Bodla, K. K.; Murthy, J. Y.; Garimella, S. V. Resistance Network-Based Thermal Conductivity Model for Metal Foams. *Comp. Mater. Sci.* **2010**, *50*, 622-632.
34. Abbas, A.; Zhao, Y.; Zhou, J.; Wang, X.; Lin, T. Improving Thermal Conductivity of Cotton Fabrics Using Composite Coatings Containing Graphene, Multiwall Carbon Nanotube or Boron Nitride Fine Particles. *Fibers and Polymers* **2013**, *14*, 1641-1649.
35. Stanković, S. B.; Popović, D.; Poparić, G. B. Thermal Properties of Textile Fabrics Made of Natural and Regenerated Cellulose Fibers. *Polymer Testing* **2008**, *27*, 41-48.

36. Baxter, S. T. The Thermal Conductivity of Textiles. *Proceedings of the Physical Society* **1946**, 58, 105.

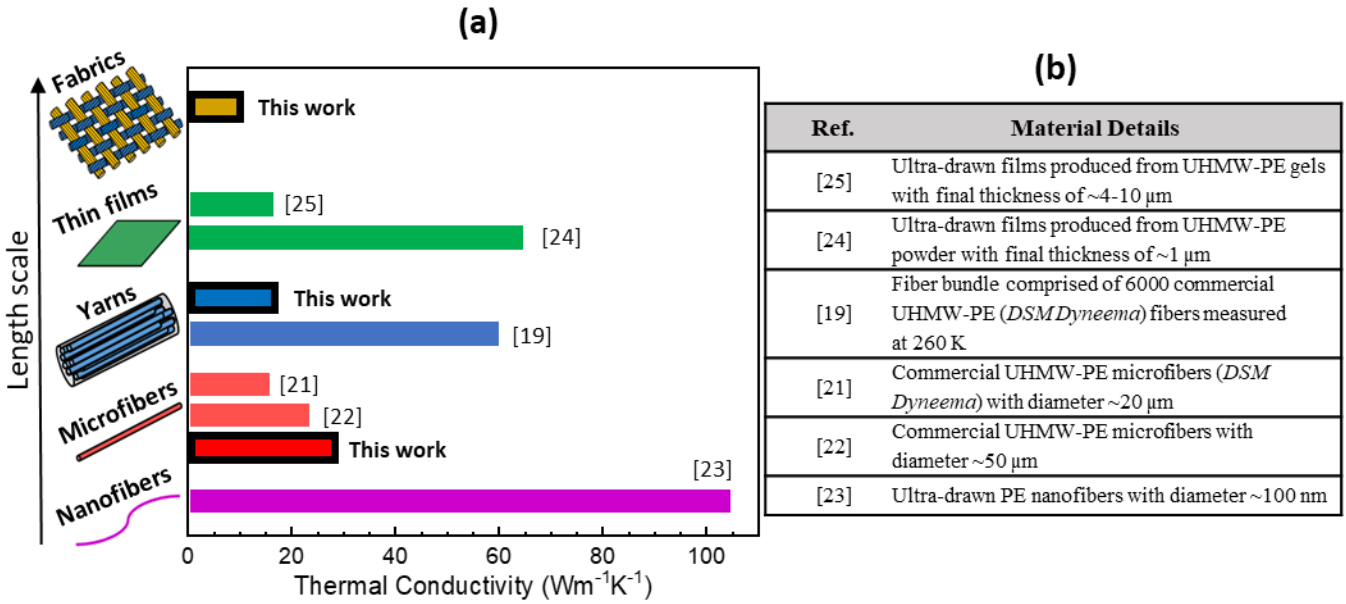


Figure 1: (a) Thermal conductivity of various forms of UHMW-PE measured in the literature and the present study. The thermal conductivity for each material is reported using a bar along the horizontal axis scale, with bars organized into groups of similar form and groups shown in order of increasing length scale. Details of the materials are listed in (b).

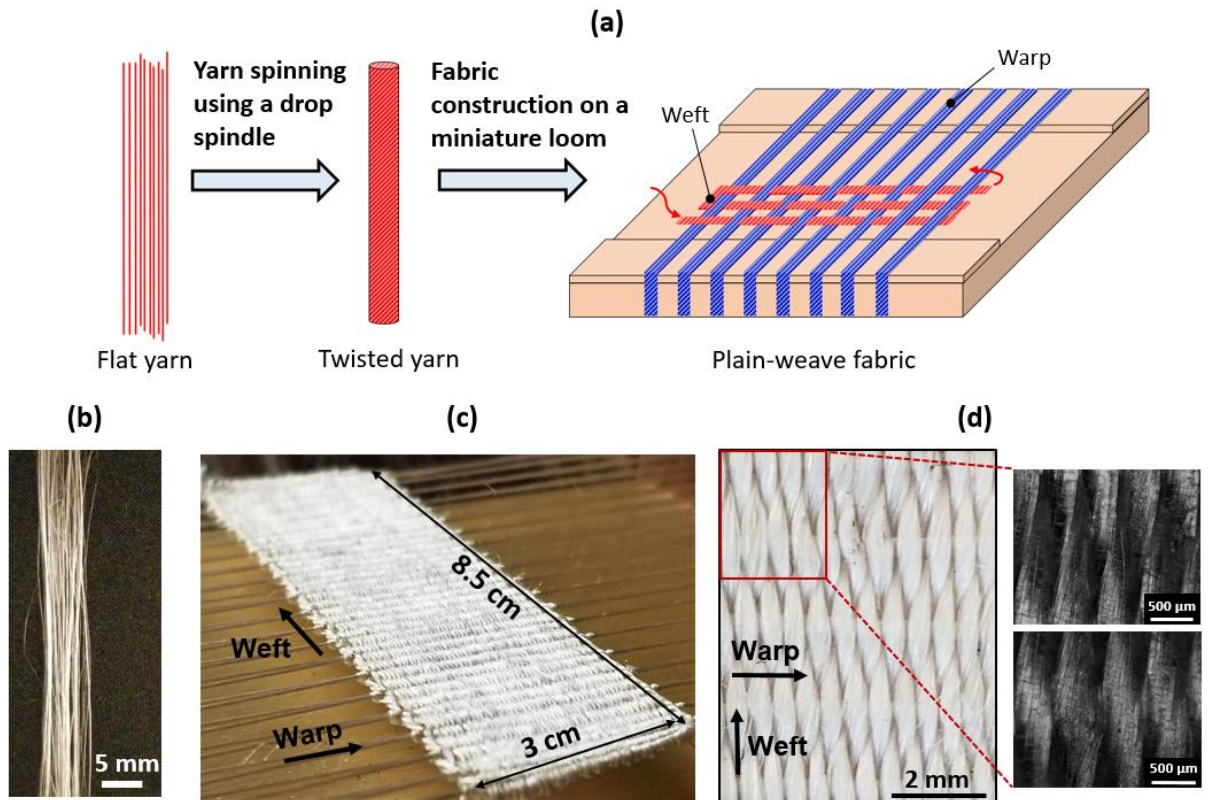


Figure 2: (a) Overview of the procedure for construction of plain-weave fabrics from flat yarn (Dyneema). Photographs of the (b) flat yarn (as received) with loosely bound individual fibers and (c) a woven fabric prototype sample when held in the miniature loom with warp and weft directions identified. (d) Top-view photograph of the woven fabric with inset showing optical microscope images of portions of the weave at high magnification. The weft yarn number density is 4-5 times higher compared to that of the warp yarns resulting in a weft-faced plain-weave pattern in which the warp is almost completely covered by the weft. Thermal characterization is conducted along the high density weft yarn direction.

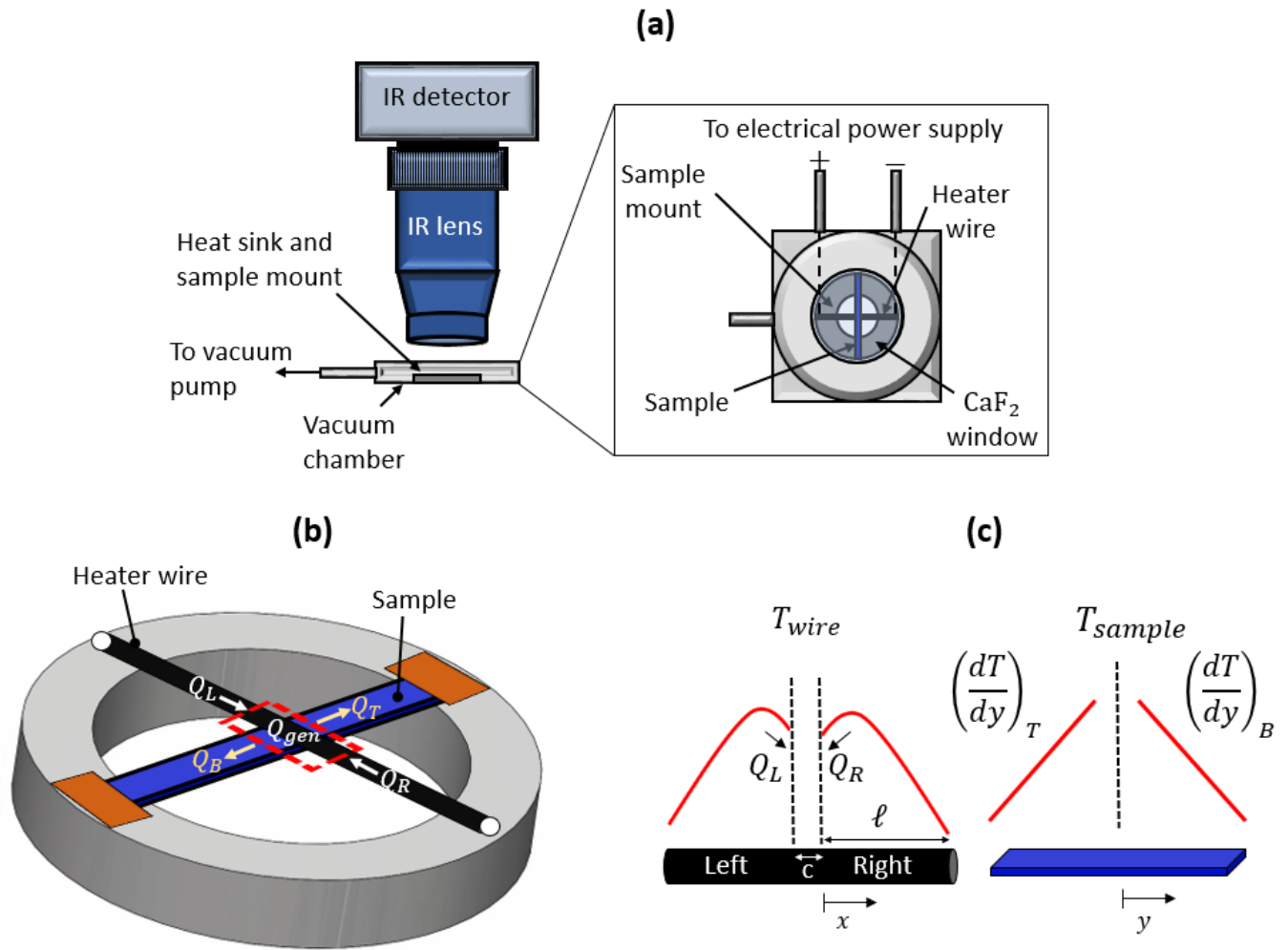


Figure 3: Schematics of the experimental setup. (a) The assembly consisting of the crossing sample and heater wire on a heat sink with a circular opening are placed in a vacuum chamber to minimize convection losses (see top-down view in inset). (b) Illustration of the energy balance in the wire–sample cross-structure arrangement; all of the heat conducted into the junction from the left and right sides of the heater wire (Q_L and Q_R , respectively) and the heat generated in the junction region (Q_{gen}) conducts into the sample (Q_T and Q_B). (c) Expected temperature profiles of the wire and the sample which are measured during the IR experiments. The heat rates (Q_L and Q_R) and temperature gradients ($(dT/dy)_T$ and $(dT/dy)_B$) are calculated from these profiles.

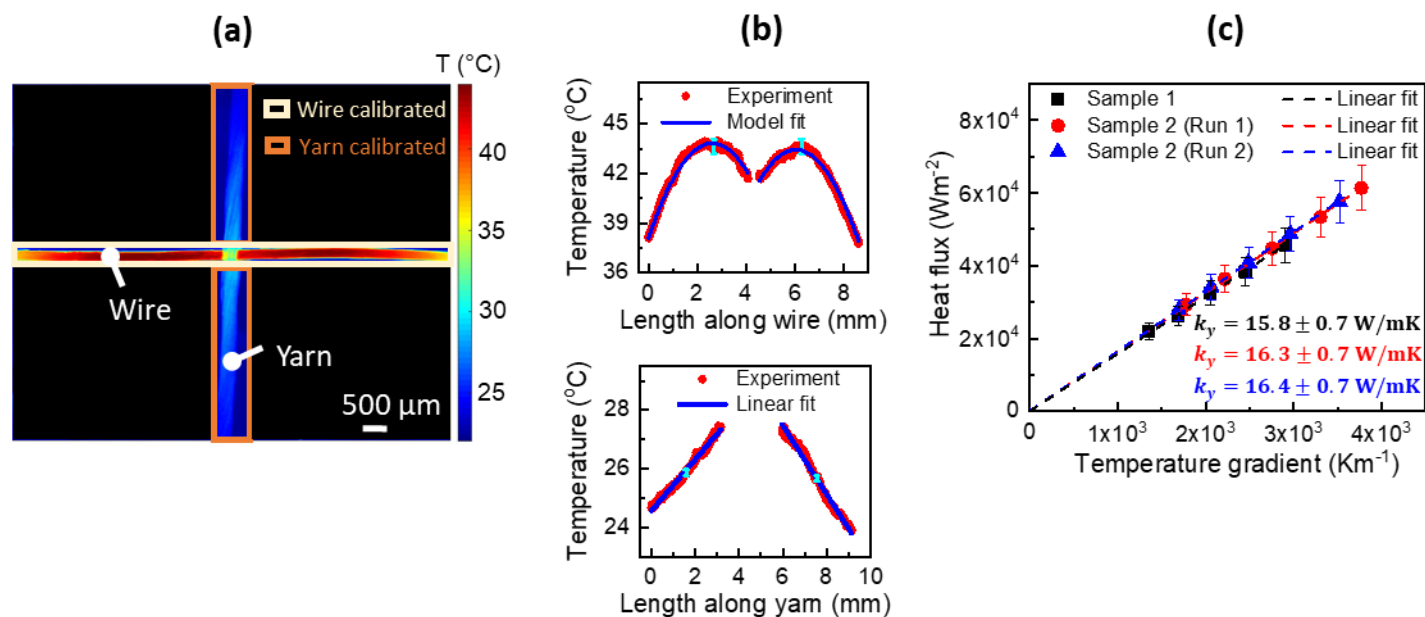


Figure 4: (a) IR temperature map of the wire–yarn experiment at a current input of 220 mA. Temperatures shown are based on corresponding emissivity values of the nichrome wire and the yarn, within the regions as indicated. (b) The corresponding temperature profiles used to extract the heat rates and sample temperature gradients are also shown. Representative error bars in the experimental temperature data are shown in cyan near the center of each profile. (c) Heat flux as a function of sample temperature gradient at different levels of input current for two different yarn samples. The slope of the linear fit across all power levels yields the thermal conductivity of the yarn sample. Error bars indicate the calculated uncertainty in heat flux and temperature gradient. Note that uncertainty in the sample temperature gradient is smaller than the data point width.

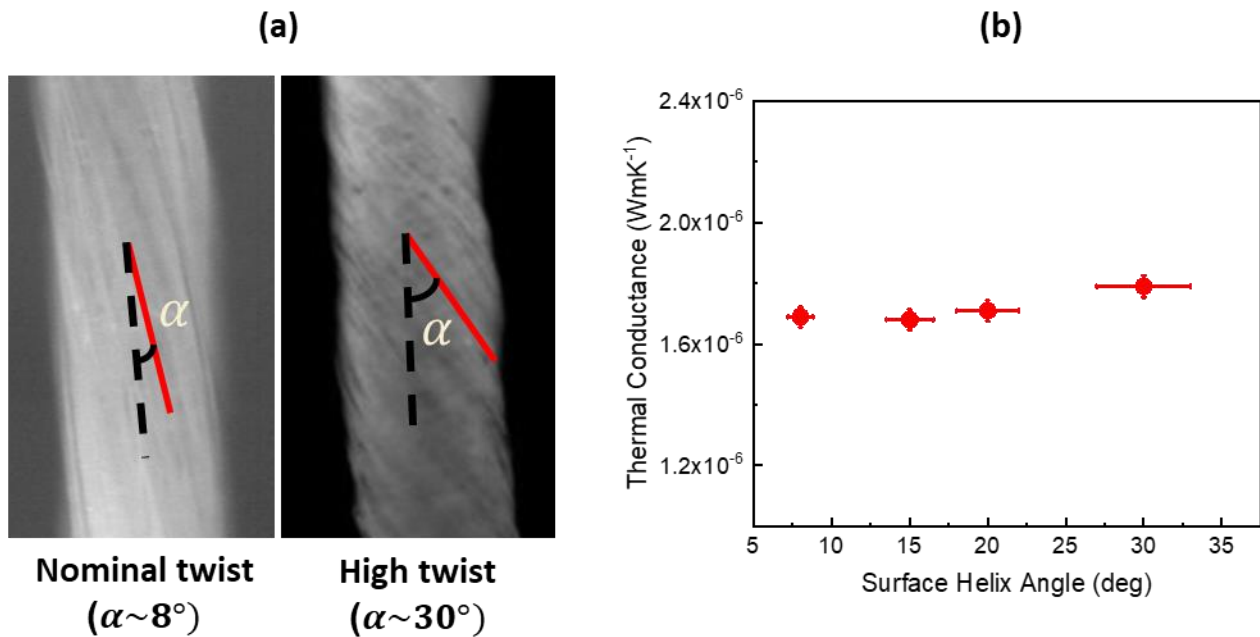


Figure 5: (a) Representative *in situ* IR images of yarns in the experimental setup at two different twist levels characterized by a surface helix angle of $\sim 8^\circ$ (low twist) and $\sim 30^\circ$ (high twist). (b) Thermal conductance (product of yarn thermal conductivity and cross-sectional area, $k_y A_y$) measured as a function of surface helix angle of the yarn. Variation of thermal conductance with twist is not very significant ($< 6\%$) for the range of twist levels evaluated.

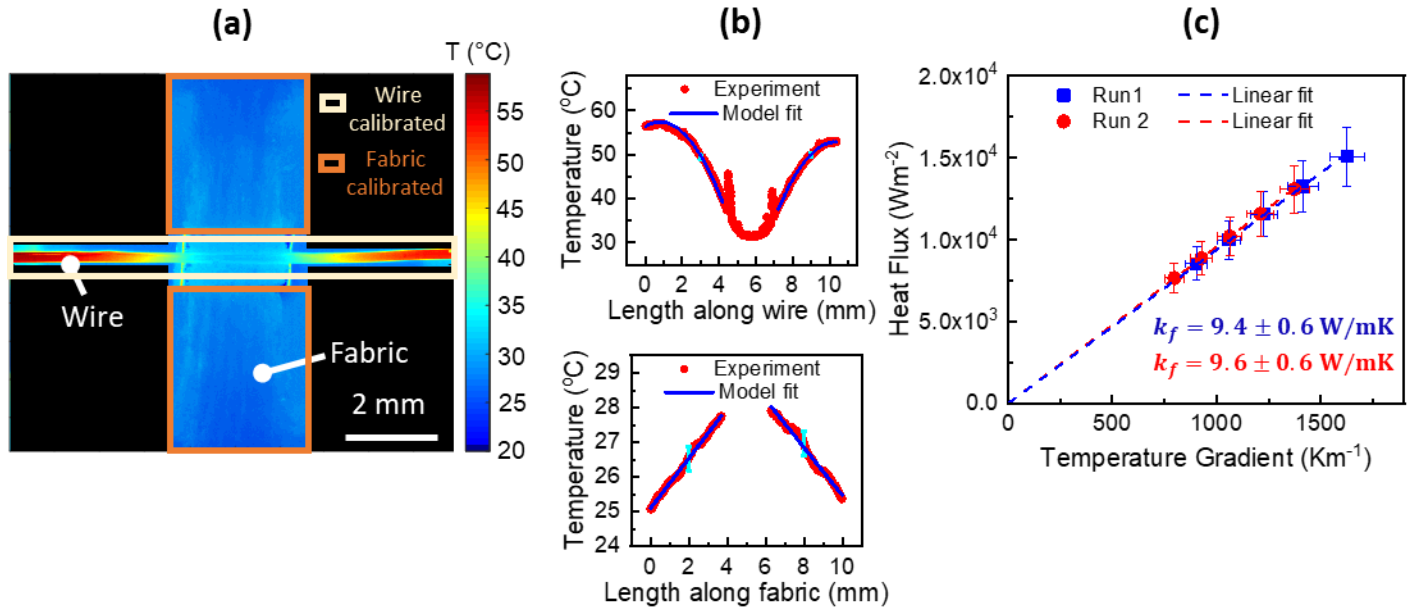


Figure 6: (a) IR temperature map of the wire–fabric experiment at a current input of 300 mA. Temperatures shown are based on corresponding emissivity values of the nichrome wire and the fabric, within the regions as indicated, and (b) the corresponding temperature profiles. Representative error bars in the experimental temperature data are shown in cyan near the center of each profile. (b) Heat flux as a function of sample temperature gradient at different levels of input current for different experimental trials: Run 1 is performed with the thermal gap pad between the wire and fabric for enhanced thermal contact, while Run 2 is performed without this pad. The slopes of the linear fit from both runs are extracted to calculate an average fabric thermal conductivity of $\sim 9.5 \pm 0.6 \text{ Wm}^{-1}\text{K}^{-1}$.

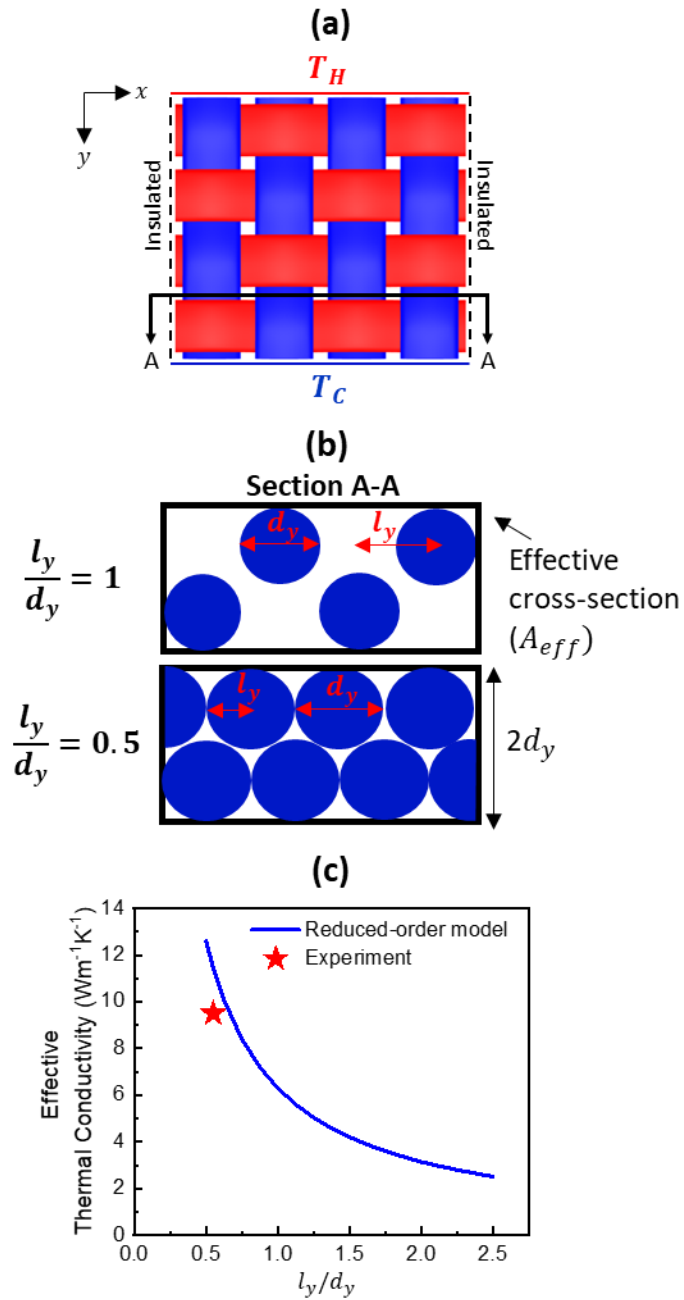


Figure 7: (a) Schematic (top-view) of a plain-weave fabric showing the boundary conditions associated with the heat transfer nodal-network model to calculate the effective thermal conductivity of the fabric in the y direction (along the blue yarns). (b) Schematic drawings of the plain-weave fabric cross-section, showing only the blue yarns that participate in heat conduction. These drawings illustrate the effective area-based packing fraction for a loose fabric ($l_y/d_y = 1$)

as compared to a tight fabric ($l_y/d_y = 0.5$). (c) Effective thermal conductivity as a function of l_y/d_y as predicted by the reduced order model. The measured fabric thermal conductivity from the experiments is shown as a 'star' symbol and agrees well with the prediction from the reduced-order model.

For Table of Contents Only

